Journal of Power Sources 199 (2012) 300–307

Contents lists available at SciVerse ScienceDirect

Journal of Power Sources

journal homepage: www.elsevier.com/locate/jpowsour

Effect of Ce-doping on the structure and electrochemical performance of lithium trivanadate prepared by a citrate sol–gel method

Zhao-jin Wu*, Yuan Zhou

Anhui Key Laboratory of Metallurgical Engineering & Resources Recycling, Anhui University of Technology, 59 Hudong Road, Maanshan 243002, PR China

ARTICLE INFO

Article history:
Received 24 August 2011
Accepted 17 October 2011
Available online 20 October 2011

Keywords:
Cathode materials
Lithium ion batteries
Lithium trivanadate
Cerium doping
Sol–gel

ABSTRACT

Ce-doped $Li_{1+x}Ce_yV_{3-y}O_8$ ($0 \le y \le 0.015$) cathode materials have been prepared through a citrate sol–gel route followed by heating at 550 °C in air. Demonstrated by XRD and elemental mapping, single-phase and homogeneous $Li_{1+x}Ce_yV_{3-y}O_8$ solid solutions are obtained at $y \le 0.01$, while $CeVO_4$ impurity presents with increasing of y up to 0.015. The $Li_{1+x}Ce_yV_{3-y}O_8$ at $y = 0.01$ delivers initial capacity of 262.33 mAh g^{-1} and capacity retention of 98.9% within the first 50 cycles, much better than the pristine $Li_{1+x}V_3O_8$ cathode (261.86 mAh g^{-1} and 87.7% accordingly). Electrochemical analyses show that an appropriate dosage of Ce can significantly suppress the capacity fading arose from lithiation phenomena around 2.55 and 2.3 V upon cycling. These interesting phenomena are mainly attributed to the stabilization of the microstructure of the material and the modification of their crystallinity and grain morphology, which lead to suppression of structural damage from the two-phase transformation around 2.55 V upon cycling and the dissolution of active material in the electrolyte on the 2.3 V phenomena.

1. Introduction

The lithium trivanadate $Li_{1+x}V_3O_8$ has been widely studied since the first mention of its interesting performance [1], and well known as a promising cathode material for rechargeable lithium ion batteries due to its high specific energy, low cost, and good rate capacity [2–4]. $Li_{1+x}V_3O_8$ has a layered structure composed of VO_6 octahedra and VO_5 distorted trigonal bipyramid units to form stable V_3O_8 sub-lattices [5], supplying as many as five lithium ions with different octahedral and tetrahedral sites between adjacent layers. The immobile lithium ions (Li(1)) fill the octahedral sites and keep the layers strongly connected, while the additional lithium ions (Li(x)) occupy the tetrahedral sites and participate in charge/discharge processes. Nevertheless, the power properties of $Li_{1+x}V_3O_8$ must be improved because only about 80% of theoretical capacity could be achieved [6], and the cyclability is still insufficient for commercial application.

Numerous researches have been devoted to improve the reversible capacity of $Li_{1+x}V_3O_8$ materials, and decreasing their grain size to reduce the transport length for both electrons and ions is one of the widely adopted methods. For achieving small grains, the soft chemical routes to prepare $Li_{1+x}V_3O_8$ precursors followed by heating at lower temperature have been generally approved. The resultant materials, however, usually exhibit undeveloped crystalline shape and lead to a significant capacity fading upon electrochemical lithiation/delithiation cycles [2,7]. This phenomenon was reported [2,7,8] to be attributed to two aspects: (1) local damage of the crystal structure arose from the two-phase transformation between $Li_3V_3O_8$ and $Li_4V_3O_8$ around 2.6 V upon cycling; and (2) the nonhomogeneous vanadium dissolution in electrolyte at the surface of the grains during the last electrochemical phenomenon around 2.3 V. They both depend strongly on the materials structure (lattice and microstructure stability, grain morphology, their size and size distribution, material crystallinity, etc.). It can thus be concluded that a modified crystal structure and appropriate grain morphology are beneficial for $Li_{1+x}V_3O_8$ materials to both reversible capacity and cyclability.

Hetero-atom doping is an effective route to improve the electrochemical behaviors of cathode materials by modifying the crystal structure [9]. Substitutions of various metal ions (Mo, Mn, W, Cr, Y, Ni, Cu, etc.) for V in $Li_{1+x}V_3O_8$ have been tried and proved effectively [10–16]. The cations with similar radius to the host ions are widely used as dopants for cathode materials because of their contribution to the electrochemical properties of the materials without severe lattice distortion. However, it is generally acknowledged that the effects of doping on the electrochemical performance of the electrode just arise from some optimization of microstructure and morphology of the active materials through addition of dopans [9]. Thus a moderate lattice distortion is acceptable for active materials if it is helpful to improve their structural

* Corresponding author. Tel.: +86 555 2311879; fax: +86 555 2311879.
E-mail addresses: wzjof@hotmail.com, wzjof@sina.com (Z.-j. Wu).

0378-7753/$ – see front matter © 2011 Elsevier B.V. All rights reserved.
doi:10.1016/j.jpowsour.2011.10.066

stability upon electrochemical cycling. From this point of a view, the dopant with obviously different ionic radius comparing to host ion should result in more modifications in the electrochemical properties of the electrode if the doping is successfully performed. As aforementioned, capacity fading of $Li_{1+x}V_3O_8$ cathode was mainly attributed to the local damage of the crystal structure resulted from repeating expansion/contraction of lattice cell due to the two-phase transformation $Li_3V_3O_8/Li_4V_3O_8$ at 2.5–2.6 V upon cycling. Trying to improve this problem, we can make an assumption that partial substitution of V^{5+} with a hetero-ion with larger radius and higher affinity for oxygen to introduce a pre-expansion of $Li_{1+x}V_3O_8$ lattice cell. These pre-expansion of initial lattice cell may restrain the damage of structure derived from repeating expansion/contraction of lattice cell upon cycling. Moreover, the stability of the host structure could be enhanced due to stronger combining power of the hetero-ion to oxygen.

Cerium (Ce) has a big radius and high affinity for oxygen, and has been reported as an effective dopant for $LiMn_2O_4$ cathode materials [17,18]. In present work, Ce^{3+} was introduced into $Li_{1+x}V_3O_8$ compound as substitutes for partial V through a citrate sol–gel method. $Li_{1+x}Ce_yV_{3-y}O_8$ ($y = 0$, 0.005, 0.01 and 0.015) has been synthesized successfully, and the effects of Ce substitution on the structure, morphology, and electrochemical properties of samples were studied in detail.

2. Experimental

The starting materials used in the experiment were lithium hydroxide ($LiOH{\cdot}H_2O$), ammonium metavanadate (NH_4VO_3), cerium acetate ($Ce(CH_3COO)_3{\cdot}5H_2O$), citric acid ($C_6H_8O_7{\cdot}H_2O$) and ammonia ($NH_3{\cdot}H_2O$), being all of analytical grade. $Li_{1+x}Ce_yV_{3-y}O_8$ compounds, where $y = 0$, 0.005, 0.01 and 0.015, were synthesized by a citrate sol–gel method as described in our previous paper [19]. Stoichiometric quantities of NH_4VO_3, $LiOH{\cdot}H_2O$ and $C_6H_8O_7{\cdot}H_2O$ were added to deionized water in turns by stirring at 60 °C on a magnetic stirring electric heater. The molar ratio of $C_6H_8O_7{\cdot}H_2O$ to total metal ions is 1.1. A few minutes later, stoichiometric amounts $Ce(CH_3COO)_3{\cdot}5H_2O$ was added into the solution while stirring. When adjusting the pH value to 7 using ammonium hydroxide, a transparent blue sol is formed. After stirring at 60 °C for 3 h, and set for 10 h, followed by the evaporation of water in a bath at 80 °C, a gel was obtained. The obtained gels were dried at 110 °C for 12 h to form xerogel precursors. Finally, $Li_{1+x}Ce_yV_{3-y}O_8$ powders were synthesized by sintering the xerogel precursor at 550 °C for 24 h in air and then cooling to room temperature.

Thermogravimetry and differential thermal analysis (TG-DTA, SDT Q600) were performed in air at a heating rate of 10 °C min^{-1} from ambition temperature to 700 °C, using α-Al_2O_3 as a reference. The structures of products were studied using X-ray diffraction (XRD, D/Max-RA, Cu Kα, Rigaku). The powder morphology was observed by scanning electron microscope (SEM, JSM-6380LV, JEOL) operating at beam voltages between 20 and 30 kV. Elemental mapping of the as-prepared $Li_{1+x}Ce_yV_{3-y}O_8$ powder was analyzed by an energy dispersive X-ray spectroscopy (Genesis 2000, JEOL).

The cathode electrodes were prepared with the active materials, acetylene black and polyvinylidene fluoride (PVDF) binder in a weight ratio of 75:15:10. Electrochemical characterization of the products was performed in cells with metallic lithium as the negative electrode, a solution of 1 M $LiPF_6$ in ethylene carbonate (EC)/dimethyl carbonate (DMC) (1:1, v/v) as the electrolyte and polypropylene microporous film (Celgard 2300) as separator. The cells were assembled in an Ar-filled glove box. Cyclic voltammetry (CV) studies at a scan rate of 0.1 mV s^{-1} and galvanostatic cycling tests at current density of 75 mA g^{-1} were made in the voltage range of 1.5–4.3 V *vs* Li, cycled at ambient temperature.

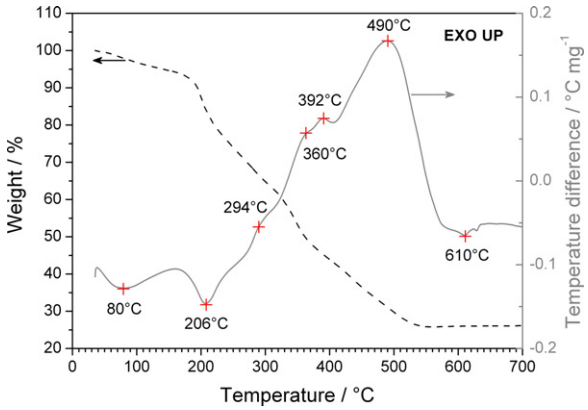

Fig. 1. TG-DTA curves of the precursor of $Li_{1+x}Ce_{0.01}V_{2.99}O_8$ prepared by sol–gel route.

3. Results and discussion

3.1. TG-DTA analysis

For determining the sintering temperature of the xerogel precursors, simultaneous TG-DTA analysis was carried out from ambition temperature to 700 °C. Experimentally, it was found that the TG-DTA curves of the precursors of $Li_{1+x}Ce_yV_{3-y}O_8$ at $y = 0$–0.015 were similar to each other. Typically, the TG-DTA curve of the precursor at $y = 0.01$ is depicted in Fig. 1.

As shown in Fig. 1, the TG-DTA curves show that the precursor could thoroughly decompose below 540 °C by several steps, accompanying with a total weight loss of 74.2%. First, evaporation of the absorbed water produces a broad endothermic peak on DTA curve around 80 °C, showing weight loss of 5.7% from ambient temperature to 160 °C. Secondly, escapes of the ammonia and crystal water from the precursor bring about an acute endothermic peak on DTA curve around 206 °C, indicating a weight loss of 17.4%. Thirdly, a multiplex exothermic effect from 260 to 540 °C produces a large complex exothermic peak on DTA curve with the tip temperature of 490 °C, corresponding to a total weight loss of 51.1%. On the left side of the complex exothermic peak, three weak exothermic peaks emerged respectively around 294, 360 and 392 °C may be caused by the decompositions of the citrate complexes into intermediates, indicating total weight loss of 31.9%. From 405 to 540 °C, the sharp exothermic peak implies an acute crystallization of the lithium trivanadate, associating with a weight loss of 19.2% owing to a thorough decomposition of the organic component. Finally, the precursor was completely converted to Ce-doped lithium trivanadate powders beyond 540 °C. When the temperature reached 610 °C, a small endothermic peak without weight loss is observed on DTA curve, which should be ascribed to the melting of Ce-doped lithium trivanadate.

It has been reported that $Li_{1+x}V_3O_8$ could form in temperature as lower as 300 °C when the precursor was prepared by citric sol–gel route [20], whereas some impurities were detected in the product prepared bellow 400 °C, and the weight loss of the precursors only stopped as temperature up to about 600 °C according to their publication. It means that a higher temperature is needed for further deposition of the citrate complexes and elimination of all the organics in the precursors. This is also demonstrated by the several exothermic peaks observed on the DTA curve from 260 to 490 °C shown in Fig. 1 of the present work. The precursor prepared through citric sol–gel route, in fact, consists of multiple citrate complexes such as $Li[V_2O_4(C_6H_5O_7)]$ and $(NH_4)[V_2O_4(C_6H_5O_7)]$ [21], accordingly thorough conversion of the

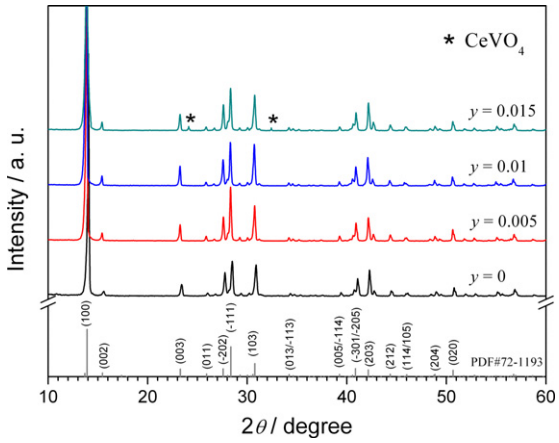

Fig. 2. XRD patterns of as prepared $Li_{1+x}Ce_yV_{3-y}O_8$ at $y = 0$, 0.005, 0.01 and 0.015, respectively.

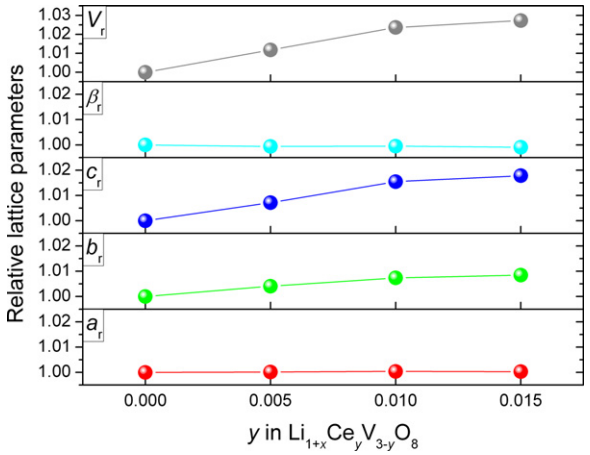

Fig. 3. Variations of lattice parameters of as prepared $Li_{1+x}Ce_yV_{3-y}O_8$ with different amount of Ce doping.

precursor to $Li_{1+x}V_3O_8$ would be dependent on complete decomposition of these intermediates. Therefore, it can be considered that the synthesis of $Li_{1+x}V_3O_8$ should proceed within a certain temperature range. Although Liu et al. reported that $Li_{1+x}V_3O_8$ was formed at 400 °C by citric sol–gel method [20], and well-developed $Li_{1+x}V_3O_8$ crystalline was obtained at 450 °C [19], the weight loss of the Ce-doped precursor was observed to stop till 540 °C in the present work. Thus the temperature for sintering the xerogel precursors was selected as 550 °C according to TG-DTA analysis in the present work.

3.2. X-ray diffraction and SEM analysis

The XRD patterns of the obtained $Li_{1+x}Ce_yV_{3-y}O_8$ ($y = 0$, 0.005, 0.01 and 0.015) are shown in Fig. 2. The diffraction peaks of the samples with different amount of Ce doping can be indexed as the monoclinic $Li_{1+x}V_3O_8$ phase with the space group $P21/m$, according to the standard pattern of PDF#72–1193. The results indicate that the as-prepared materials can form a solid solution as the formula of $Li_{1+x}Ce_yV_{3-y}O_8$ at the range of $0 \le y \le 0.01$, and there are no detectable impurity phases in the powders synthesized by the citric sol–gel method. When y increased to 0.015, an impurity phase was present, exhibiting two weak peaks ($2\theta = 24.04°$ and 32.42°) ascribed to $CeVO_4$ (marked by asterisks) according to PDF#12–0757. These phenomena imply that only a small quantity of cerium ions could be alloyed into $Li_{1+x}V_3O_8$ owing to a strong difference in ionic radius between cerium and vanadium, so that excessive addition of cerium (e.g. $y = 0.015$) should lead to the impurities in the samples. In addition, the XRD patterns also show that the intensities of the main diffractive peaks of Ce-doped samples are stronger than that of the pristine $Li_{1+x}V_3O_8$ sample, hinting the effect of Ce-doping on structure of the material.

The effect of the doping ions on the acceptor structure is also identified by the increase in the position shift of the (1 0 0) peak towards lower 2θ angles shown in Fig. 2. This phenomenon suggests that Ce doping leads to lattice expansion of $Li_{1+x}V_3O_8$ cell.

Table 1
Refined lattice parameters of as-prepared $Li_{1+x}Ce_yV_{3-y}O_8$ synthesized by the citric sol–gel method.

y	a (Å)	b (Å)	c (Å)	β (°)	V (Å^3)
0	6.659(2)	3.599(9)	12.009(2)	107.662(5)	274.33
0.005	6.660(3)	3.614(7)	12.095(2)	107.598(2)	277.57
0.010	6.661(7)	3.626(5)	12.195(3)	107.609(9)	280.81
0.015	6.661(3)	3.630(5)	12.223(4)	107.565(3)	281.82

The lattice parameters of the samples calculated by XRD data are listed in Table 1. It shows obvious changes in the lattice parameters of $Li_{1+x}Ce_yV_{3-y}O_8$ as y increases from 0 to 0.015. For clarity, the relative cell parameters a_r, b_r, c_r and β_r, as well as cell volume (V_r), which are defined as $a_r = a_y/a_0$, $b_r = b_y/b_0$, $c_r = c_y/c_0$, $\beta_r = \beta_y/\beta_0$ and $V_r = V_y/V_0$, respectively, are used to describe the changes in lattice parameters and plotted in Fig. 3. It can be seen that the increases in b, of about 0.41%, 0.74% and 0.85%, and in c, of about 0.72%, 1.55% and 1.78%, are observed when y increased from 0 to 0.005, 0.01 and 0.015, respectively. On the other hand, the changes in a and β values are inconspicuous. As a result, the cell volume V increases from 274.33 to 277.57, 280.81 and 281.82 Å when y increased from 0 to 0.005, 0.01 and 0.015, respectively, indicating that a pre-expansion in lattice cell of $Li_{1+x}Ce_yV_{3-y}O_8$ were induced by Ce doping.

Note that the lattice parameters b and c increase almost linearly with increase of y from 0 to 0.01. Whereas, their increase get slowly when y further increase from 0.01 to 0.015, which may arise from the formation of the impurity phases $CeVO_4$ at $y = 0.015$. In addition, the increase in c is steeper than that in b value with increase of Ce doping, hinting a selective expansion of V_3O_8 sublattices because of partial substitution of V with Ce. The parameter a is associated with the interlayer distance ($d_{100} = a \sin\beta$) [11], so the interlayer distance increases slightly as y is increased. This may be derived from a buffer effect, which is provided by the interstitial space between adjacent vanadate chains, against partial doping-swell. A similar phenomenon was reported by Arumugam and Kalaignan on the investigation of $LiCe_xMn_{2-x}O_4$ [18]. It has been confirmed that the abrupt lattice expansion/contraction of $Li_{1+x}V_3O_8$, which resulted from electrochemical cycles over two-phase boundary, is responsible for the local damage of the crystal structure [7,8]. It induces a loss of contact between some grains and the carbon black, compromising the electronic internal path of the composite electrode and producing a subsequent loss of capacity. In view of the above, the pre-expansion of lattice cell caused by Ce doping may provide more lattice space for lithium ion intercalation/deintercalation, and then alleviate the amplitude of reciprocating changes in cell parameters resulted from subsequent electrochemical processes. Consequently, an improved cycliability for $Li_{1+x}Ce_yV_{3-y}O_8$ electrode could be expected.

Fig. 4 shows SEM images of the $Li_{1+x}Ce_yV_{3-y}O_8$ ($y = 0$, 0.005, 0.01 and 0.015) powders. The pristine $Li_{1+x}V_3O_8$ sample appears as a mixture of some large plate-like crystals and large numbers of smaller particles with undeveloped crystalline shape (Fig. 4a), exhibiting a wide size distribution. The largest platelet had its longest side as long as 50 μm and the smallest particle had its longest side less than 1 μm. By contrast, the Ce-doped samples

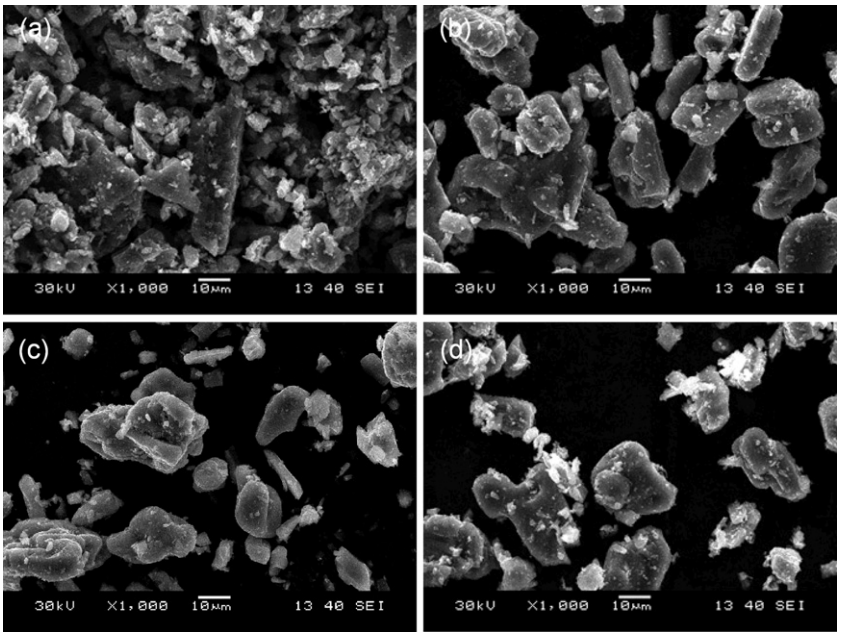

Fig. 4. Typical SEM images of as-prepared $Li_{1+x}Ce_yV_{3-y}O_8$ at $y = 0$ (a), 0.005 (b), 0.01 (c) and 0.015 (d), respectively.

appear as almost granules of 10–20 μm with well solid crystal shape (Fig. 4b–d). Moreover, the plate-like grains show gradual decrease in dimension with the increase of Ce doping and disappear at $y = 0.015$. It means that the shape anisotropy of the grains is weakened by addition of Ce, while the crystallinity and size distribution of the grains are improved because of Ce doping. The results suggest that Ce doping would disturb the preferential growth of the $Li_{1+x}V_3O_8$ crystals, inducing a morphological evolution of the $Li_{1+x}Ce_yV_{3-y}O_8$ grains into granular shape. Note that the granular grains of the Ce-doped $Li_{1+x}V_3O_8$ show a homogeneous size distribution and well developed crystalline than that of the pristine $Li_{1+x}V_3O_8$, being consistent with the changes in diffraction peak intensity observed on the XRD patterns. In addition, the decrease in amount of small grains with undeveloped crystal shape would prevent them from dissolution in the electrolyte [7]. These all hint the improvement on cyclic behavior of $Li_{1+x}V_3O_8$ electrode by Ce doping.

Fig. 5 shows the elemental mapping of as-prepared $Li_{1+x}Ce_yV_{3-y}O_8$ at $y = 0.01$. The distribution areas for elements Ce are homogeneous. It demonstrates that the dopants had achieved homogeneous solid solution with the material, being well agreeable to the result of XRD analyses.

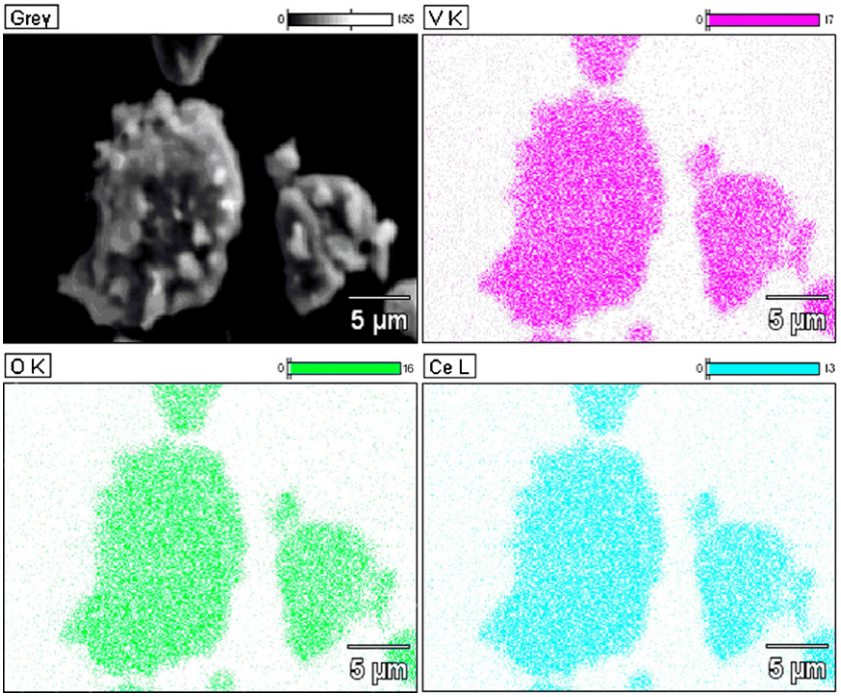

Fig. 5. Elemental mapping of as-prepared $Li_{1+x}Ce_yV_{3-y}O_8$ ($y = 0.01$).

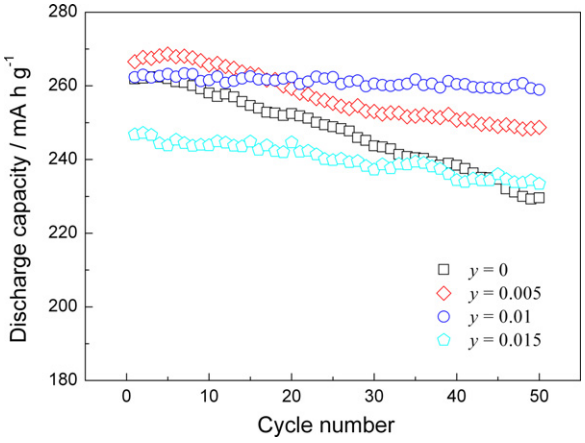

Fig. 6. Changes in cycling performance of $Li_{1+x}Ce_yV_{3-y}O_8$ with different amount of Ce doping.

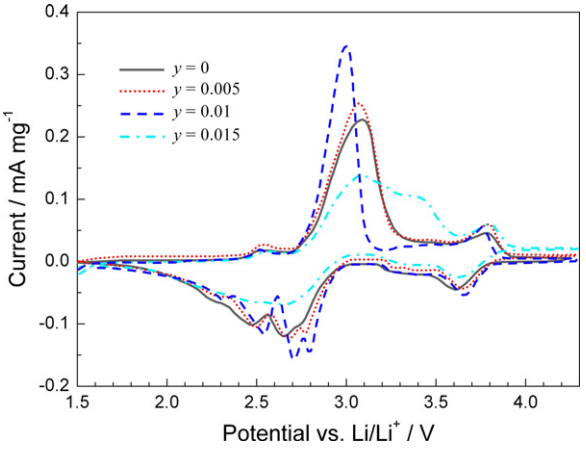

Fig. 7. The 2nd cyclic voltammograms of $Li_{1+x}Ce_yV_{3-y}O_8$ cathodes ($y = 0$, 0.005, 0.01 and 0.015).

3.3. *Electrochemical performances of the synthesized* $Li_{1+x}Ce_yV_{3-y}O_8$

Galvanostatic charge/discharge tests and cyclic voltammetry studies on $Li_{1+x}Ce_yV_{3-y}O_8$ ($y = 0$, 0.005, 0.01 and 0.015) cathodes were performed to evaluate the effects of Ce doping on electrochemical behaviors of lithium trivanadate.

Fig. 6 shows the discharge capacities for $Li_{1+x}Ce_yV_{3-y}O_8$ at current density of 75 mA g^{-1} in the voltage range 1.5–4.3 V. It can be seen that the pristine sample ($y = 0$) delivered an initial capacity of 261.86 mAh g^{-1} and a capacity retention of 87.7% at the end of the 50th cycle. In contrast, the samples doped by cerium exhibited the initial capacity of 266.55, 262.33 and 246.79 mAh g^{-1} at $y = 0.005$, 0.01 and 0.015, and their capacity retentions at the end of the 50th cycle were found to be 93.3%, 98.9% and 94.6%, respectively. The results indicate that the dose of cerium has a remarkable effect on the initial capacity and cyclic behavior of $Li_{1+x}Ce_yV_{3-y}O_8$ in the range of $0 \le y \le 0.015$.

Comparing to the initial capacity of the pristine $Li_{1+x}V_3O_8$ sample, those of Ce-doped samples exhibit a slight waves (within 5 mAh g^{-1}) at $y = 0.005$ and 0.01, whereas it presents an abrupt drop by 15.07 mAh g^{-1} at $y = 0.015$. These phenomena may arise from the effects of grain morphologies (size and size distribution) on the initial capacity of the active materials. It has been reported that solid crystals with large grain size gave rise to a low capacity because their bulk was not accessible for Li insertion within the time allowed for the tests [2]. Our pristine $Li_{1+x}V_3O_8$ consists of a few large plates and lots of small particles. The large plates actually account for a considerable mass percentage, which leads to a decrease in initial capacity due to a kinetic limitation despite the fact that lots of small particles are accessible for Li insertion. On the other hand, the Ce-doped samples are composed of almost all the granular solid crystals with moderate dimensions and more homogeneous size distribution than the pristine one, nearly without the large plates. These may be the cause of the difference in the initial capacity among $y = 0$, 0.005 and 0.01 samples. The bigger initial capacity loss for $y = 0.015$ sample may arise from the formation of $CeVO_4$ impurity detected by XRD analysis in Fig. 2.

The capacity retention upon 50 cycles of the testing electrodes demonstrates a strong improvement on the cyclic performance of the samples by Ce doping in present experiment. Especially, the sample of $y = 0.01$ has the best cyclic performance and the highest mean capacity among three Ce-doped samples. It is known that the factors influencing the cyclability mainly relate to the crystal shape (well formed crystals or not) [2] and lattice distortion upon electrochemical cycles [5,7,8]. The undoped sample has lots of small grains with undeveloped crystal shape and tends to react with the electrolyte, leading to partial dissolution at the surface and detriment to cyclability. On the contrary, the Ce-doped samples possess well-developed solid crystals, which suppress the surface reactivity of grains to electrolyte and result in a good cyclability. In addition, the drastic changes in lattice parameters upon cycling through two-phased phenomenon at 2.6 V leads to local damage of the crystal structure, which has been demonstrated to be the main cause of the capacity fading of pristine $Li_{1+x}V_3O_8$. The Ce-doped samples, however, exhibit the mild pre-expansion in lattice cell as mentioned in Section 3.2, may be beneficial to the cyclability. When y increased to 0.015, the formation of $CeVO_4$ impurity may be responsible for the decrease in capacity retention as well as initial capacity, suggesting that the addition of cerium at $y = 0.015$ is too excessive to achieve the excellent electrochemical behaviors (cyclability and initial capacity).

In order to further discuss the effects of Ce doping on the electrode reactions of $Li_{1+x}Ce_yV_{3-y}O_8$ materials, CV tests were carried out in the voltage range of 1.5–4.3 V *vs* Li at a scan rate of 0.1 mV s^{-1}. The 2nd CV curves of the $Li_{1+x}Ce_yV_{3-y}O_8$ cathodes are depicted in Fig. 7. Because the pristine testing cells were directly discharged from open circuit voltage to 1.5 V at the beginning of CV tests, the 1st CV curves are unclosed and not plotted here.

For the undoped sample, five peaks observed in the cathodic scan from 4.3 to 1.5 V correspond to lithium insertion in sites with energy differences for holding of Li^+ ions [5,22]. The peaks around 3.6, 2.8, and 2.7 V represent the electrochemical signature of single-phase reactions with lithium ions occupying the tetrahedral sites, and that around 2.55 V is related to the intercalation of lithium ions for octahedral sites resulting in a two-phase transformation between $Li_3V_3O_8$ and $Li_4V_3O_8$ [2,5,7,23], while the last peak around 2.3 V concerns a slower kinetic insertion process representing the electrochemical signature of single-phase reaction with all lithium ions occupying the octahedral sites [3,8,24]. The cathodic peaks around 2.55 V was considered as the origin of capacity fading during the cycling of LiV_3O_8 due to some local damages of the crystal structure in electrochemical lithiation/delithiation processes. The 2.3 V peak was reported to be associated with the dissolution of small quantity of V^{3+} in the electrolyte [7], also resulting in capacity fading upon cycling.

In the case of the Ce-doped samples, the cathodic peaks between 3.0 and 2.0 V exhibit enhancement in current density and slight shift of peaks position towards the higher potential side with increase of Ce doping till $y = 0.01$, and the anodic peak around 3.0 V shows an amplification in current density also but shift of peak position towards the lower potential side, revealing that

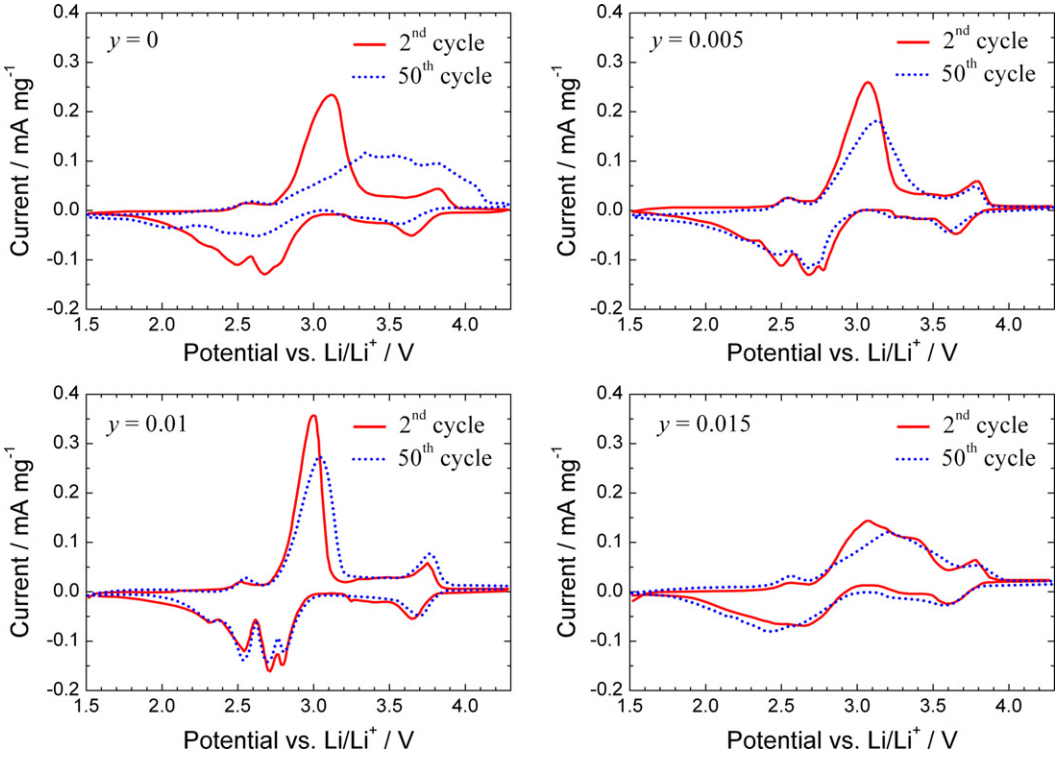

Fig. 8. Comparison of the 2nd CV and 50th cyclic voltammograms of $Li_{1+x}Ce_yV_{3-y}O_8$ cathodes ($y = 0$, 0.005, 0.01 and 0.015).

the crystallinity of the active materials and kinetics for Li^+ insertion/extraction were improved by Ce doping. When $y = 0.015$, however, an abrupt drop in current density occurs to both cathodic and anodic peaks, and a new anodic peak is present around 3.4 V. These phenomena indicate that only small dose ($y \leq 0.01$) of Ce doping could effectively be alloyed into the $Li_{1+x}V_3O_8$ and improve the kinetics of electrochemical reactions for the electrodes. Further increasing the addition of Ce to $y = 0.015$ resulted in formation of impurities such as $CeVO_4$ and structural destroy upon cycling, leading to a decline in electrochemical performance. Remarkably, the cathodic peaks at 2.55 and 2.3 V are gradually enhanced with increasing of y from 0 to 0.01, meaning that the structural destroy and partial dissolution of V^{3+} pieces in the electrolyte upon prolonged electrochemical cycles should be suppressed by Ce doping. To further evaluate the effects of these issues on cyclic behaviors of the electrodes, the comparisons of the 2nd and 50th CV curves are depicted in Fig. 8.

For the undoped sample shown in Fig. 8, the CV curve of the 50th cycle is rather different from that of the 2nd cycle. The changes in redox peaks on CV curves from the 2nd to 50th mainly include considerable fading of current density of redox peaks and significant shift of anodic peak position to the higher potential side. Furthermore, the major anodic peak around 3.0 V on the 2nd CV curve split into three peaks around 3.5 V on the 50th CV curve. These results indicate that some irreversible structural changes occurred during cycling which lead to diminution of electrode material available for electrochemical reaction [25]. As for the samples with addition of Ce from 0.005 to 0.01, both fading of current density and right-shift of anodic peak position are evidently suppressed within 50 cycles. Especially, the CV curves of $Li_{1+x}Ce_{0.01}V_{2.99}O_8$ are nearly reproducible from the 2nd to 50th cycles except for slight decrease in current density of anodic peak around 3.0 V, suggesting more excellent reversibility of Li^+ ions transport in its bulk and through its interface with the electrolyte than those for the samples of $y = 0$ and 0.005. When the addition of Ce to 0.015, the CV profiles from the 2nd to 50th cycles still remain well reproducible, aside from slight reduction of peak current densities. These phenomena suggest that the reversibility of $Li_{1+x}Ce_yV_{3-y}O_8$ can remarkably be improved with increasing of Ce doping till $y = 0.010$, further increase of Ce addition resulted in the presence of impurities such as $CeVO_4$ and leaded to fading of electrochemical capacity.

Fig. 9 shows the charge/discharge voltage profiles of $Li_{1+x}Ce_yV_{3-y}O_8$ cathodes in the 1st, 2nd and 50th cycles. In order to emphasize the details of the charge/discharge voltage profiles (i.e. *Q*–*V* curves), the plots of differential capacity *vs* voltage (d*Q*/d*V vs V*) converted from Fig. 9 were illustrated in Fig. 10. The plateaus in the *Q*–*V* plots (Fig. 9) were then transformed into peaks in the d*Q*/d*V vs V* plots (Fig. 10). The sharp peaks on the d*Q*/d*V vs V* plots indicate that the lithium insertion/deintercalation proceeds through a few multiphase regions until the limit for reversible lithium uptake is reached [26].

As shown in Fig. 9, for the charge curves of the pristine and each doped samples, no obvious difference in curve profiles can be observed between the 2nd and 50th cycles except for some changes in capacity. For the discharge curves, however, effect of Ce doping on the voltage profiles upon prolonged cycling is much remarkable. There are seven discharge plateaus located at about 3.6, 2.8, 2.7, 2.55, 2.43, 2.3 and 1.65 V present in the 1st discharge curves for each sample, which respectively correspond to the cathodic peaks at corresponding voltage on d*Q*/d*V vs V* curves in Fig. 10. It is noted that the 2.43 and 1.65 V plateaus emerged only in the 1st cycle for all samples and disappeared in the rest cycles, and moreover, the very blurry 2.55 V plateau in the 1st cycle evolved into the long and well-defined one in the 2nd and 50th cycle. These phenomena can be clearly observed from the changes in cathodic peaks of the d*Q*/d*V vs V* curves in Fig. 10, where both the strong peak at 2.43 V and the weak peak at 1.65 V in the 1st cycle have disappeared in the 2nd and 50th cycles, and the very weak peak at 2.55 V in the 1st cycle

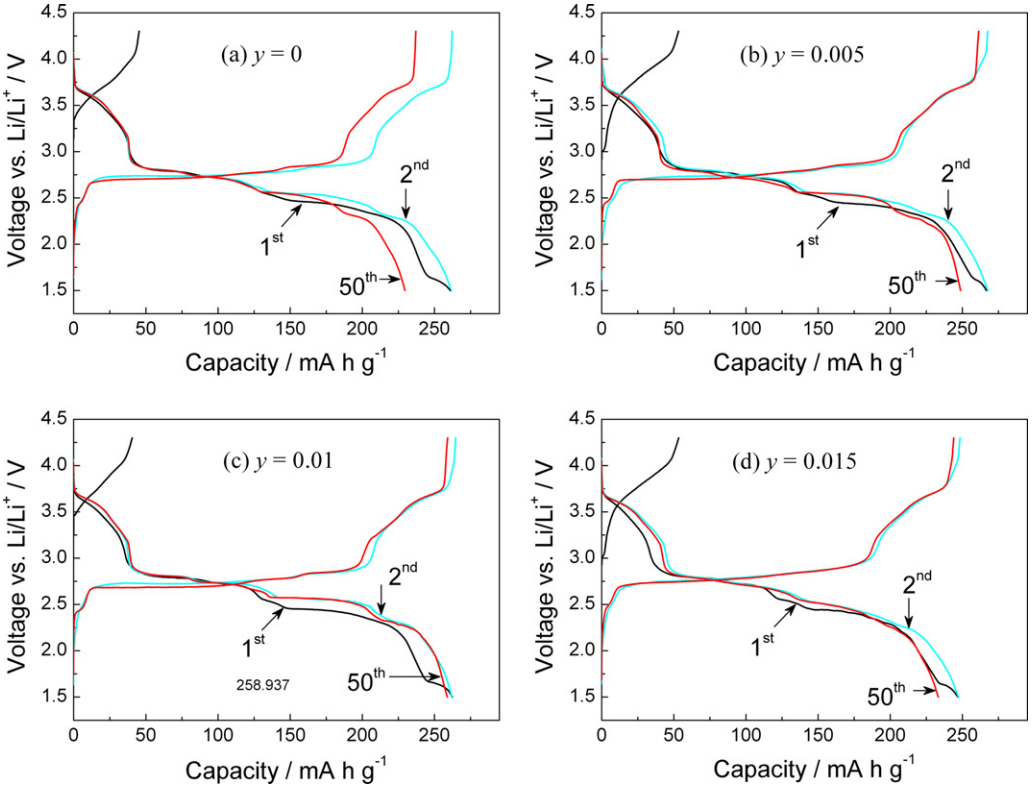

Fig. 9. Galvanostatic charge/discharge voltage profiles of $Li_{1+x}Ce_yV_{3-y}O_8$ cathodes at (a) $y = 0$, (b) 0.005, (c) 0.01 and (d) 0.015 for the 1st, 2nd and 50th cycles. Conditions: current density, 75 mA g^{-1}; voltage range, 1.5–4.3 V; room temperature.

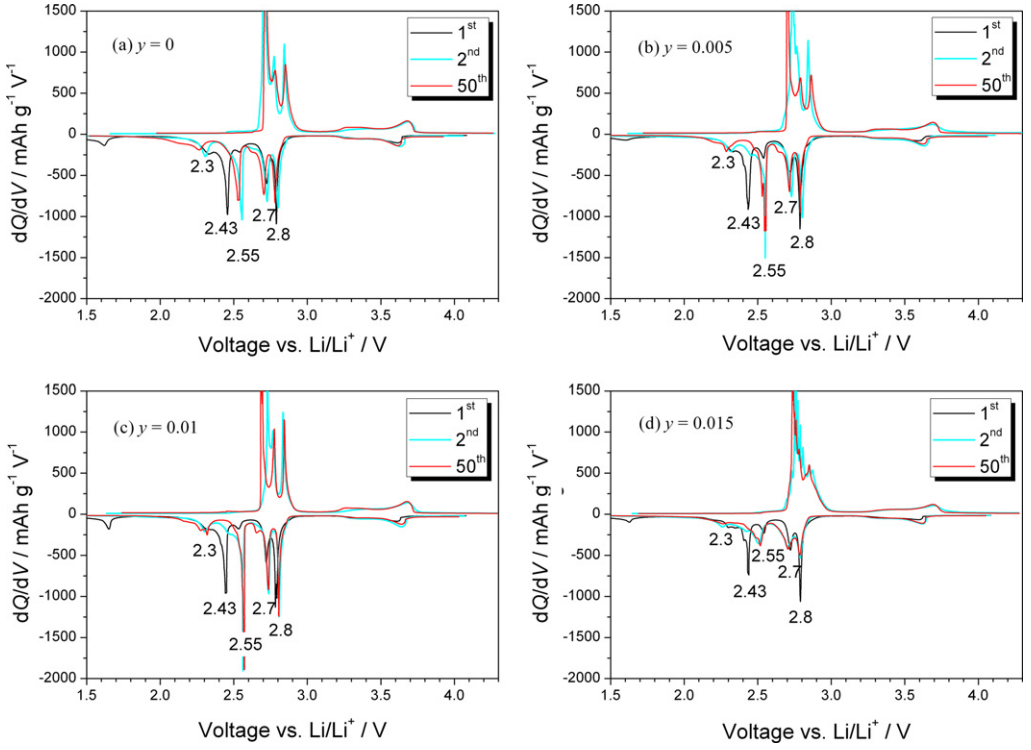

Fig. 10. Comparison of differential capacity *vs* voltage of $Li_{1+x}Ce_yV_{3-y}O_8$ cathodes at (a) $y = 0$, (b) 0.005, (c) 0.01 and (d) 0.015 for the 1st, 2nd and 50th cycles. Conditions: current density, 75 mA g^{-1}; voltage range, 1.5–4.3 V; room temperature.

turned much strong in the 2nd and 50th cycles. The results imply that microstructural changes may occur to $Li_{1+x}Ce_yV_{3-y}O_8$ during the 1st cycle. Since the 2nd cycle, four well-defined plateaus at 2.8, 2.7, 2.55 and 2.3 V are observed on discharge voltage profiles of $Li_{1+x}Ce_yV_{3-y}O_8$ cathodes, which are consistent with the cathodic peaks of the CV curves discussed in Fig. 8. It is noted that the effects of Ce doping on reversibility of $Li_{1+x}Ce_yV_{3-y}O_8$ cathodes could be estimated from the changes in their charge/discharge voltage profiles between the 2nd and 50th cycles in Fig. 9, especially from the dQ/dV *vs* V curves in Fig. 10.

Comparing the discharge voltage profiles between the 2nd and 50th cycles for the undoped sample, we can find that the plateaus of 2.8 and 2.7 V in the 50th cycle respectively show nearly the same profiles to those in the 2nd cycle, whereas the length of the 2.55 V plateau in the 50th cycle is much shorter than that in the 2nd cycle. These phenomena indicated that the capacity fading of the $Li_{1+x}V_3O_8$ is mainly produced in the two-phase transformation $Li_3V_3O_8$–$Li_4V_3O_8$ at about 2.55 V, which are in accordance with the results reported by Jouanneau et al. [7]. The finally single-phase reaction for $Li_5V_3O_8$ at about 2.3 V, another origin of capacity fading of $Li_{1+x}V_3O_8$, is found inducing a slight shrinkage in plateau length from the 2nd to 50th cycle. It may be ascribed to the presence of some undeveloped crystals in pristine sample (Fig. 4a), leading to partial dissolution of V^{3+} in the electrolyte. Accordingly, those Li ion insertion reactions at 2.55 and 2.3 V lead to a capacity fading of 32.5 mAh g^{-1} for the undoped sample within 50 cycles in the present experiment. These phenomena can also be clearly observed from the changes in cathodic peaks of the dQ/dV *vs* V curves in Fig. 10a. The cathodic peaks at 2.8 and 2.7 V exhibit similar intensity between the 2nd and 50th cycles, while those at 2.55 and 2.3 V are subjected to notable intensity drop from the 2nd and 50th cycles.

Similarly to the case of undoped sample, the Ce doped samples also presented steady discharge plateaus at 2.8 and 2.7 V on the Q–V curves, remaining almost unchanged from the 2nd to 50th cycles. However, the 2.55 V plateau of discharge curve for $Li_{1+x}Ce_yV_{3-y}O_8$ samples becomes well-defined gradually with increasing of Ce addition from 0.005 to 0.01 comparing to that for the undoped sample (Fig. 9), and the best status is observed at $y = 0.010$. The $Li_{1+x}Ce_{0.01}V_{2.99}O_8$ sample exhibits the strongest cathodic peak at 2.55 V among all tested samples, with nearly constant intensity from the 2nd to 50th cycle (Fig. 10). In the meantime, the 2.3 V plateau of the Q–V curve is also elongated by Ce doping of $y = 0.005$ and 0.01, which also contribute to improvement on cycliability of the cathode. When the addition of Ce is increased to 0.015, however, only 2.8 V plateau presents on the Q–V curve without evident plateaus at 2.7, 2.55 and 2.3 V, leading to decrease in both initial capacity and cycliability. These results indicate that appropriate substitution of Ce for V could prevent $Li_{1+x}V_3O_8$ from capacity fading around 2.5 and 2.3 V discharge. Accordingly, the discharge capacity retentions of $Li_{1+x}Ce_yV_{3-y}O_8$ cathodes for $y = 0$, 0.005 and 0.01 were increased from 87.7% to 93.3% and 98.9% upon cycling to the 50th cycle, respectively. The possible reason can be attributed to three aspects. Firstly, partial substitution of Ce ions for V ions could result in an pre-expansion of $[V_3O_8]^{-(1+x)}$ lattice cell (listed in Table 1), and consequently reduce the amplitude of expansion/contraction of lattice cell during the two-phase transformation $Li_3V_3O_8$/$Li_4V_3O_8$ around 2.55 V, being effective for the active material to counteract structure damage when it undergoes two-phase transformation. Secondly, moderate substitution of Ce could improve the crystallinity, dimensional uniformity and morphology of $Li_{1+x}V_3O_8$ grains, thus reasonably avoiding its capacity fading during the last phase transformation around 2.3 V. Finally, increasing Ce addition up to $y = 0.015$ results in the presence of impurities such as $CeVO_4$, and leaded to fading of reversible capacity.

4. Conclusion

Cathode materials $Li_{1+x}Ce_yV_{3-y}O_8$ ($0 \le y \le 0.015$) were successfully synthesized through a citrate sol–gel route followed by heating at 550 °C in air. The XRD patterns and elemental mapping suggest that cerium ions could partly substitute for vanadium ions in $Li_{1+x}V_3O_8$, and single-phase $Li_{1+x}Ce_yV_{3-y}O_8$ materials could be obtained at $y \le 0.01$.

Appropriate substitution of cerium for vanadium could significantly improve the cycliability of $Li_{1+x}V_3O_8$ without obvious decrease in initial capacity. The $Li_{1+x}Ce_{0.01}V_{2.99}O_8$ delivered initial discharge capacity of 262.33 mAh g^{-1} and capacity retention of 98.9% after fifty cycles, while the pristine $Li_{1+x}V_3O_8$ exhibited 261.86 mAh g^{-1} and 87.7% respectively. Further increasing the addition of cerium up to $y = 0.015$ leaded to decrease in initial capacity and slight drop in cycliability again. The main reason for the good cycliability of $Li_{1+x}Ce_yV_{3-y}O_8$ materials is attributed to that a suitable Ce doping could induce some pre-expansion of lattice cell of the material without presence of any detectable impurity, which can effectively counteract the structural damage originated from two-phase transformation around 2.55 V upon cycling. In addition, the cerium doping improves the crystallinity and grain morphology of $Li_{1+x}V_3O_8$ materials and suppresses the dissolution of active material in the electrolyte on the 2.3 V phenomena, which advances the cycliability of the materials.

Acknowledgements

This work was financially supported by the Anhui Provincial Natural Science Foundation (No. 11040606M105). The experimental support from the Innovation Group of Anhui University of Technology was also acknowledged.

References

[1] S. Panero, M. Pasquali, G. Pistoia, J. Electrochem. Soc. 130 (1983) 1225–1227.
[2] S. Jouanneau, A. Le Gal La Salle, A. Verbaere, M. Deschamps, S. Lascaud, D. Guyomard, J. Mater. Chem. 13 (2003) 921–927.
[3] A. Sakunthala, M.V. Reddy, S. Selvasekarapandian, B.V.R. Chowdari, P.C. selvin, J. Phys. Chem. C 114 (2010) 8099–8107.
[4] H.M. Liu, Y.G. Wang, W.S. Yang, H.S. Zhou, Electrochim. Acta 56 (2001) 1392–1398.
[5] L.A. de Picciotto, K.T. Adendorff, D.C. Liles, M.M. Thackeray, Solid State Ion. 62 (1993) 297–307.
[6] F. Tanguy, J. Gaubicher, D. Guyomard, Electrochim. Acta 55 (2010) 3979–3986.
[7] S. Jouanneau, A. Le Gal La Salle, A. Verbaere, D. Guyomard, J. Electrochem. Soc. 152 (2005) A1660–A1667.
[8] J. Kawakita, Y. Katayama, T. Muria, T. Kishi, Solid State Ion. 107 (1998) 145–152.
[9] J.W. Fergus, J. Power Sources 195 (2010) 939–954.
[10] J. Kawakita, H. Katagiri, T. Miura, T. Kishi, J. Power Sources 68 (1997) 680.
[11] S.V. Pouchko, A.K. Ivanov-Schitz, F.G.B. Ooms, J. Schoonman, Solid State Ion. 144 (2001) 151–161.
[12] Y. Feng, Y.L. Li, F. Hou, Mater. Lett. 63 (2009) 1338–1340.
[13] C.Q. Feng, L.F. Huang, Z.P. Guo, J.Z. Wang, H.K. Liu, J. Power Sources 174 (2007) 548–551.
[14] Y.W. Tian, X.X. Kang, L.Y. Liu, C.Q. Xu, T. Qu, J. Rare Earths 26 (2008) 279–283.
[15] L. Liu, L.F. Jiao, J.L. Sun, M. Zhao, Y.H. Zhang, H.T. Yuan, Y.M. Wang, Solid State Ion. 178 (2008) 1756–1761.
[16] X.Y. Cao, C. Yuan, L.L. Xie, H. Zhan, Y.H. Zhou, Ionics 16 (2010) 39–44.
[17] R. Thirunakaran, A. Sivashanmugam, S. Gopukumar, R. Rajalakshmi, J. Power Sources 187 (2009) 565–574.
[18] D. Arumugam, G.P. Kalaignan, J. Electroanal. Chem. 648 (2010) 54–59.
[19] Z.J. Wu, X.B. Zhao, J. Tu, G.S. Cao, J.P. Tu, T.J. Zhu, J. Alloy Compd. 403 (2005) 345–348.
[20] L. Liu, L.F. Jiao, Y.H. Zhang, J.L. Sun, L. Yang, Y.L. Miao, H.T. Yuan, Y.M. Wang, Mater. Chem. Phys. 111 (2008) 565–569.
[21] F. Wu, L. Wang, C. Wu, Y. Bai, Electrochim. Acta 54 (2009) 4613–4619.
[22] J. Kawakita, M. Majima, T. Miura, T. Kishi, J. Power Sources 66 (1997) 135–139.
[23] F. Bonino, S. Panero, M. Pasquali, G. Pistoia, J. Power Sources 56 (1995) 193–196.
[24] H.M. Liu, Y.G. Wang, K.X. Wang, Y.R. Wang, H.S. Zhou, J. Power Sources 192 (2009) 668–673.
[25] A. Esmanski, G.A. Ozin, Adv. Funct. Mater. 19 (2009) 1–12.
[26] C.Q. Feng, S.Y. Chew, Z.P. Guo, J.Z. Wang, H.K. Liu, J. Power Sources 174 (2007) 1095–1099.